Green synthesis of thin shell carbon-encapsulated iron nanoparticles via hydrothermal carbonization

Blanca Calderon, Fraser Smith, Ignacio Aracil, and Andrés Fullana

ACS Sustainable Chem. Eng., **Just Accepted Manuscript** • DOI: 10.1021/acssuschemeng.8b01416 • Publication Date (Web): 25 Apr 2018

Green synthesis of thin shell carbon-encapsulated iron nanoparticles via hydrothermal carbonization

B. Calderon[a,*], *F. Smith*[a], *I. Aracil*[a], *A. Fullana*[a]

*blanca.calderon@ua.es, Tel:+34965903400 , X. 2920

[a]Chemical Engineering Department, University of Alicante, San Vicente del Raspeig Road, s/n 03690 San Vicente del Raspeig, Alicante, Spain

ABSTRACT

Nanoscale zero valent iron (nZVI) has proven to be a promising solution for contaminant remediation, but its application is limited due to its high cost of synthesis and instability. Encapsulating the nZVI in carbon spheres generates more stable particles with improved properties due to the adsorption capacity provided by the carbon. The aim of this work was to synthesize thin shell carbon-encapsulated iron nanoparticles (CE-nFe) through hydrothermal carbonization (HTC) using olive mill wastewater as a carbonaceous source, which is a cheaper and more sustainable method of synthesis than current practice. With this method, a high quality nanomaterial was obtained, which displayed surface areas up to 220 m^2/g and was composed of ~4 nm iron nanoparticles spheres surrounded by a thin layer of carbon (<1 nm). The effect of HTC conditions on the nanoparticles structure and morphology was evaluated. Post-treatment of the samples under nitrogen flow at high temperatures (600-800ºC) was used to increase the ZVI content of the samples. Finally, the synthesized CE-nFe were tested for the removal of heavy metals from water. Thanks to the carbon layer, CE-nFe proved to avoid the delivery of heavy metals ions back to water, a behavior previously observed with nZVI due to its aging after long time periods.

Keywords

nZVI, olive mill wastewater, encapsulation, HTC, green chemistry, heavy metal removal, aging, waste valorization

INTRODUCTION

Nanoscale zero valent iron (nZVI) particles have proven in the last two decades to be a powerful tool for water treatment.[1] Their interest lies in their capacity to remove a wide range of pollutants through the donation of electrons in reduction processes, but also through the adsorption of contaminants in its oxide shell[2]. nZVI has proven to be effective at the reductive dehalogenation of chlorinated compounds, the sequestration of heavy metals, and the degradation of organic dyes, among others [3]. However, its use in environmental remediation is limited due to its lack of stability and easy aggregation in micro size flocs.[4] Due to its extremely reactive surface, nZVI also reacts with dissolved oxygen and water, which accelerates the nanoparticles aging and results in a loss of reactivity towards not target compounds. Agglomeration of nZVI takes place via Van der Waals forces, electric dipolar interactions and most importantly, by magnetic forces among the nanoparticles, causing either a reduction in their effective surface area and/ or a decrease in its reactivity. Another important problem that is limiting the practical application of nZVI is its high cost of production. The most common method for nZVI synthesis is the reduction of ferrous salts by sodium borohydride, which is driven at ambient temperature and pressure.[5] However, the process is expensive and is not feasible for large-scale implementation, due to the large volume of hydrogen gas generated in the reaction and the high cost of borohydride salt.[6] Moreover, sodium borohydride is a toxic reagent. As a result, large-scale production of commercial nanoparticles is being conducted mainly by high temperature reduction of iron oxides in hydrogen atmosphere.[7] This method, although being more easily scalable, involves high capital costs. Other alternative methods such as grinding, ultrasound and electrochemical methods are currently being developed.[8]

Considering the sequestration of heavy metal cations, one of the barriers for the application of nZVI is the presence of an "aging effect". As shown in a previous work[9], although the initial uptake of heavy metals by nZVI is good, as time elapses the nZVI releases some of the heavy metal cations back into water due to the nZVI aging. Research conducted by Crane et al.[10]

showed that coating iron nanoparticles with carbon reduced the release of uranium back to water due to the retention effect of carbon.

In order to counteract the drawbacks of nZVI current application, the encapsulation of nZVI is being studied with the objective of enhancing the stability of nZVI without sacrificing its efficiency in contaminant remediation.[11] The encapsulation of nZVI inside micro or nano-carbon spheres via hydrothermal carbonization (HTC) using an organic compound as carbonaceous source, such as glucose or sucrose, has been recently developed.[12] HTC consists of a thermal treatment of an aqueous solution or dispersion of a carbon-containing organic material at moderate temperature and under autogeneous pressure, which produces a carbon-rich solid as an insoluble product.[13] This method is easily scalable since is endothermic and generates only gaseous products.[14] It is considered a green method for nZVI synthesis, because it does not use toxic reactants. Furthermore, when using a waste as the carbon-source material the method becomes even more environmentally friendly. The carbon-encapsulated iron nanoparticles (CE-nFe) obtained show improved capability for contaminant removal due to the combination of the reducing properties of iron and the adsorptive capacity of the carbon.[15]

Spain is the main world producer of olive oil with a 37.5% of the total production worldwide.[16] According to Azbar et al.[17], the waste generation in the olive oil industry is nearly the 75% of the total mass harvested, which entails a high impact on the environment due to its high phytotoxicity. One of the waste streams from the olive oil production is the olive mill wastewater (OMW), which is rich in carbonaceous compounds, including polyphenols.[18] Previous studies have indicated that tea extracts, which also contain polyphenols, can be used to synthesize iron nanoparticles at room temperature. According to the literature, polyphenols and other natural compounds such as caffeine not only act as capping agents that minimize the oxidation and agglomeration of zero valent iron, but also serve as reducing agent for the synthesis of this metallic iron.[19-22] The chelating nature of polyphenols appears also in the literature in other fields of research.[23,24] Considering this, OMW was used as a feedstock in this

work to produce CE-nFe through HTC, making profit of its reducing and capping properties to maximize the amount of nZVI and the percentage of iron in the final material.

The aim of this work has been to develop a cheaper and more sustainable method for the synthesis of CE-nFe from OMW and investigate its application to heavy metal removal. Different conditions, such as iron to carbon ratio in the raw material, and heating temperature and time, were assessed. A post-treatment of the nanomaterial to increase its nZVI content was also investigated. This synthesis method could help dealing with the waste from the olive oil industry, and at the same time would produce a high quality nanomaterial able to treat polluted water sources.

MATERIALS AND METHODS

Chemicals

OMW was obtained from an olive mill company from Extremadura region in Spain, and was used after being clarified by centrifugation at 5000 rpm during 30 min and filtration with an 8 μm fiber glass filter. The other reagents used, $Ni(NO_3)_2 \cdot H_2O$, $Cd(CH_3COO)_2 \cdot 2H_2O$, $ZnCl_2$, $K_2Cr_2O_7$, $CuCl_2 \cdot H_2O$, $Fe(NO_3)_3 \cdot 9H_2O$ (Sigma-Aldrich), $FeSO_4 \cdot 7H_2O$ (VWR), zinc powder (Fischer Scientific), ethanol (Montplet) and 37% HCl (Fischer Scientific), were of analytical grade. All the solutions were prepared using purified water.

CE-nFe synthesis

The experimental procedure followed was based on Sun et al.'s work[6], in which iron (III) nitrate nonahydrate is reduced by means of a hydrothermal reaction with glucose. However, the glucose was replaced by olive mill wastewater and slight modifications were performed. Briefly, 300 mL of clarified OMW were mixed with 0.057 mol of $Fe(NO_3)_3 \cdot 9H_2O$ for 1 h. Then, the mixture was transferred to a 1 L HTC reactor (FCF-1 from Zhengzhou Keda Machinery) and was submitted to the required temperature and time (see Table 1). After cooling down the

reactor with water at 5-10ºC, the resulting mixture was filtered under vacuum with a 0.2 μm cellulose acetate filter and washed 2 times with a 50/50 (v/v) ethanol water solution. Subsequently, the solid fraction was transferred to an oven and dried at 80ºC during 12 h. The sample was then ground into a fine powder and transferred to a vial for characterization.

Table 1 shows a summary of the different conditions studied for CE-nFe. Note that the experiment P1 was conducted without iron, as a reference for subsequent analyses. In the experiment P3, glucose was used instead of OMW to compare both materials as the carbonaceous source to produce the CE-nFe. In order to ensure equal comparison between both experiments, a solution was made with glucose to contain the same level of total organic carbon (TOC) as the OMW. In the rest of the experiments, HTC temperature was varied between 180 and 275ºC and HTC reaction time from 0.5 to 18 h. The ratio of iron to carbon was also changed by varying the amount of iron nitrate nonahydrate and maintaining the amount of OMW constant.

Table 1. Reaction conditions of HTC synthesis of CE-nFe and main properties of the nanomaterial obtained.

Sample	Carbon source	T (ºC)	Reaction time (h)	nFe/nC$_i$[1] (molFe/molC)	Solid weight (g)	$w_{Total\ Fe}/w_{Sample}$ (%)	$w_{Fe(0)}/w_{Total\ Fe}$ (%)	Surface area (m^2/g)
P1	OMW	200	3	0	1.0	-	0.0	3.6
P2	-	200	3	-		67.4	2.9	53
P3	Glucose	200	3	0.05	7.6	5.5	38.6	11
P4	OMW	200	3	0.05	7.5	42.5	9.6	176
P6	OMW	180	3	0.05	7.9	36.9	6.5	108
P7	OMW	225	3	0.05	7.4	44.5	5.5	190
P8	OMW	250	3	0.05	7.3	44.2	3.5	169
P9	OMW	275	3	0.05	7.1	44.8	6.8	146
P10	OMW	200	0.5	0.05	8.1	37.8	13.8	130
P11	OMW	200	18	0.05	7.1	43.9	6.8	149
P12	OMW	200	3	0.01	4.1	19.3	11.4	22
P13	OMW	200	3	0.025	6.3	26.0	6.3	46
P14	OMW	200	3	0.1	11.0	52.6	5.6	134

P15	OMW	200	3	0.150	14.9	58.8	4.3	94
P16	OMW	200	3	0.2	16.9	65.1	4.0	71
P17	OMW	200	3	0.25	24.3	65.2	4.5	79

[1] nC_i (initial carbon molar amount of the sample) was calculated from the COT value of the OMW. nCi = COT(mg/L)·V· M_w^{-1} where V is the volume of OMW and M_w its molecular weight.

Subsequently, the samples were thermally treated at high temperatures (600-800ºC) under anaerobic conditions in order to increase their zero-valent iron content (post-treatment). Specifically, the samples were inserted into a quartz tube and treated in an oven during 3 h under a nitrogen mass flow of 500 mL/min. Then, the samples were extracted by adding distilled water after cooling the sample to room temperature in order to avoid its ignition with air. The samples were labeled as CE-nFe-P600, CE-nFe-P700 and CE-nFe-P800 for post-treatment temperatures of 600, 700 and 800ºC respectively.

Analysis methods

OMW was characterized by calculating its total organic carbon (TOC) by difference of total carbon (TC) and inorganic carbon (IC) measured using a TOC-5000A from Shimadzu. In order to obtain the solid fraction of the OMW, the sample was heated in an oven at 105ºC during 8 h. Then, elemental analysis was performed by grinding it into a fine powder and analyzing it with an Elemental Microanalyzer Thermo Finningan Flash 1112 Series in order to determine the percentage of C, N, H and S. pH measurement was performed using a Mettler Toledo Seven Multi using the electrode 5014 of Crison. ICP-OES was performed to obtain the concentration of the main elements of the OMW after digesting the sample with nitric acid and hydrogen peroxide.

Field emission scanning electron microscopy (FESEM) performed on a Merlin VP Compact from Zeiss at a voltage of 1 kV was used to evaluate the size, morphology and iron distribution in the CE-nFe. Transmission electron microscopy (TEM) with a JEOL JEM-2010 was used to determine the size of the iron nanoparticles and its location within the carbonaceous structure. The software Infinity Analize from Lumenera was used to measure the size of the nanoparticles.

The Brunauer-Emmet-Teller (BET) surface area and the pore size distribution of the samples were obtained by physical adsorption with nitrogen at 77 K, using a Mark Quantachrome Autosorb-6. Prior to the measurements, the samples were degassed under vacuum at 200ºC for 4 h. X-ray diffraction (XRD) was performed to determine the crystalline structure of the samples using a Bruker D8-Advance with CuKα radiation at 40 kV and a step size of 0.05º 2θ at 3 s/step.

The iron content and thermal stability of the samples were determined by thermogravimetric analysis (TG) under air or nitrogen with a Perkin Elmer Thermobalance model TGA/SDTA-6000. The amount of iron incorporated into the CE-nFe was calculated by heating the sample to 950ºC under air, which entails the combustion of carbon and the oxidation of iron to Fe_3O_4. The ash at 950ºC was assumed to be the amount of iron oxide plus the rest of inorganic compounds, the latter being calculated by heating the sample P1 (without iron) at 950ºC.

The zero valent iron (Fe^0) content was determined by measuring the volume of H_2 gas produced during the digestion of 0.1 g of the sample with 1 mL of 37% HCl, which is proportional to the amount of iron, as shown in equation 1. Specifically, the sample is located in a vessel which is communicated with a water column in a graduated burette. A known volume of HCl is added to the vessel through a septum, and the H_2 gas produced causes the displacement of the water column. The difference between the initial and final height of the water column corresponds to the H_2 gas produced plus the volume of HCl added (1 mL). On the basis of the standard reduction potentials, the iron oxides do not produce H_2 when acidified. The soundness of the method was determined by measuring the H_2 generated by a known sample of Zn. The difference between the observed and theoretical value was less than 10% for 6 repetitions of the measurement.

$$2Fe + 6HCl \rightarrow 2FeCl_3 + 3H_2 \qquad (1)$$

Application of CE-nFe particles on heavy metal removal of contaminated water

The synthesized CE-nFe, CE-nFe-P600 and conventional nZVI particles were tested for the treatment of an aqueous solution containing 10 ppm of the following heavy metals: Cu, Zn, Cr, Ni and Cd, which are commonly found in ground and wastewater. The solution was prepared synthetically using the corresponding reagents enumerated in the "Chemicals" section. Furthermore, a carbon sample synthesized by HTC from OMW without iron addition and submitted to post-treatment (AC-P600) was tested for heavy metal removal under the same conditions. The aim of this experiment was to determine the influence of the carbon in heavy metal removal.

Experiments were performed in a 500 mL batch laboratory scale reactor under continuous mixing with a magnetic stirrer. The volume of contaminated solution used in each experiment was 500 mL. A specific amount of nanomaterial was added to the reactor to start the reaction, and 2 mL samples were taken from the solution at various reaction times. The nanoparticles were separated from the solution by using a neodymium magnet, followed by centrifugation. The concentration of the heavy metal cations in water was determined using inductively coupled mass spectrometry (ICP-MS) using a VG PQ-ExCell from Thermo Elemental prior filtration with PTFE 0.2 μm syringes and acidification to 2% of nitric acid.

RESULTS AND DISCUSSION

Comparison between OMW and glucose as a feedstock for CE-nFe synthesis

The characteristics of the OMW used for the synthesis of CE-nFe are shown in Table S1 and S2 of Supporting Information and are similar to those reported for OMW in other works, having a high organic carbon content and an acidic pH[25,26].

The results from the characterization of the materials synthesized by glucose and OMW revealed significant differences between them. For the same synthesis conditions, glucose CE-nFe (G-CE-nFe) exhibited only 5.5% of incorporation of Fe in the solid (see Table 1), compared to 42.5% of Fe content achieved when using OMW as a feedstock (OMW-CE-nFe). Additionally, the iron content in OMW-CE-nFe was significantly higher than that obtained by

other authors using glucose as a raw material. For example, in Sun et al.'s work [6], 10.5% iron content was obtained using the same initial molar ratio of Fe/C, and in Yu et al.'s work[27] only 7.4% of iron was incorporated into the material for a Fe/C initial molar ratio four times higher. Interestingly, the analysis of zero valent iron content revealed that iron present in G-CE-nFe was in a higher extent metallic iron (38.6% of total iron compared to only 9.6% for the OMW-CE-nFe). However, although the glucose was able to produce a higher percentage of zero valent iron, as the total iron incorporated in the sample was much lower, it resulted in a Fe^0 content in G-CE-nFe (2.2%) half of the value displayed by OMW-CE-nFe (4.5%). Therefore, it is reasonable to assume that olive mill wastewater, which is known to be rich in polyphenols, is significantly more reducing than glucose, thus incorporating more metallic iron into the final carbonaceous structure [28].

The iron distribution in the materials was evaluated by using the signal of the backscattered electrons in FE-SEM. It was not possible to observe the iron in the G-CE-nFe samples with this technique, in accordance with the low iron percentages detected in this sample (see Table 1). Conversely, as shown in Figure S1 of Supporting Information, OMW-CE-nFe displayed a very good distribution of iron through the material.

Concerning the morphology and size of the materials obtained, TEM and FE-SEM images of the particles were evaluated (see Figure 1). Both materials showed to have a completely different morphology. While G-CE-nFe consisted of micro-spheres of diameters of 2.0 ± 0.7 μm, OMW-CE-nFe presented a sphere-like nanostructure of sizes of 130 ± 50 nm (see Figure S2 in Supporting Information), which were composed of smaller spheres of iron nanoparticles of very small size (4.4 ± 0.6 nm) surrounded by a thin layer of carbon (<1 nm). OMW-CE-nFe displayed strong aggregation, as expected for particles synthesized by HTC method. The smaller size and more porous structure of OMW-CE-nFe provide the material with a higher surface area and better properties for contaminant remediation compared to G-CE-nFe.

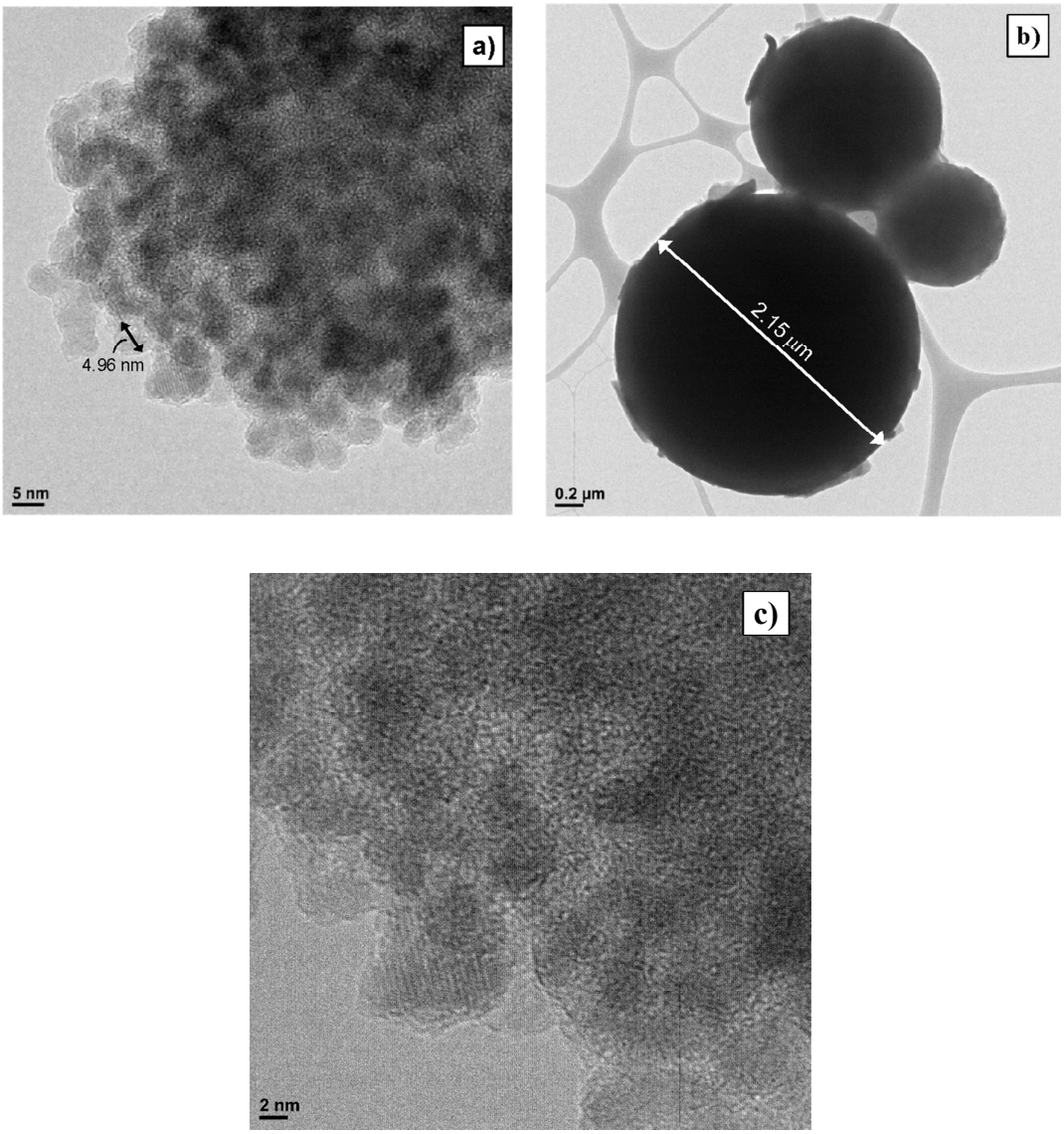

Figure 1. TEM images of: a) OMW-CE-nFe (sample P4), b) G-CE-nFe (sample P3), c) HRTEM image of the nanoparticles shell of OMW-CE-nFe (sample P4). Reaction conditions: 200ºC, $nFe/nC_i = 0.05$, 3 h

N_2 adsorption isotherms of both samples were evaluated and BET surface area and pore size distribution using the Barret-Joyner-Halenda (BJH) method were calculated (see Figure S3 in Supporting Information). The adsorption isotherms were both of type IV, suggesting a mesoporous structure in accordance with the IUPAC classification of isotherms. Both isotherms presented a type H3 hysteresis loop, which indicated the presence of slit-shaped pores. The available BET surface area of OMW-CE-nFe was around 15 times higher than that of G-CE-nFe

(176 m^2/g vs 11 m^2/g). Thus, although the OMW-CE-nFe showed strong aggregation, similar to what is observed for conventional nZVI, its surface area was much greater than that of nZVI (7.1 m^2/g), probably due to the lower size of the encapsulated nanoparticles and to the carbon layer. Similarly, the pore volume of OMW-CE-nFe was of 0.59 cm^3/g, which is much higher than the one of G-CE-nFe (0.027 cm^3/g), further evidencing the different structure between both materials.

With regard to the pore size distribution, G-CE-nFe showed a wider distribution of pores in the sample, centered at 3.3, 4.2, 5.9 and 16.3 nm. Conversely, OMW-CE-nFe displayed a single modal pore size distribution centered at 3.8 nm. Most probably, the pore size detected for OMW-CE-nFe was attributed to the inter-particle voids. In order to obtain the size of the intra-particle pores, the density functional theory (DFT) analysis could be useful. Nevertheless, this model has to be regarded only as a semi-quantitative evaluation of the pore size distribution, as none of the models available describes an activated carbon with iron content higher than 40%. The quenched solid density functional theory (QSDFT) was applied with a kernel of an activated carbon containing slit pores to the desorption branch of the isotherm (see Figure S4 in Supporting Information). Results showed that, additionally to the pore size of 3.4 nm, pores at 1.2 and 1.8 nm which pertain to the supermicropore region were detected. Thus, it is reasonable to conclude that OMW-CE-nFe have also some pores in the micropore region, although their calculated size should be taken as an approximate value.

Regarding the crystalline composition of both materials, there were significant differences between them, as showed by XRD pattern (see Figure S5 in Supporting Information). In OMW-CE-nFe only the crystalline phase γ-Fe_2O_3 was detected, while in G-CE-nFe, the characteristic peaks from iron oxide and iron carbide were identified. Moreover, also nitrogen-containing compounds were identified ($(C_5H_9NO_4)_n$ and $C_2H_5NO_4H_2O$), which were ascribed to the presence of nitrate in the reaction medium. This indicated that when using glucose as a raw material, the solid obtained had more than one crystalline phase. Conversely, OMW-CE-nFe

were more homogeneous, presenting only one crystalline phase ascribed to the iron oxide, while carbon was amorphous and did not participate in any crystalline phase.

Summarizing, the material obtained using OMW as a feedstock demonstrated to have a structure very different from that of G-CE-nFe. OMW-CE-nFe were composed of nanocarbon spheres, instead of the common microspheres of 6-8 μm which are obtained when glucose or sucrose are used as a feedstock[6,22], presented a higher surface area and a greater incorporation of iron into the material. The differences between G-CE-nFe and OMW-CE-nFe could be attributed to the different composition of both raw materials. In the case of OMW, a wide range of different compounds, such as diverse polyphenols, organic acids, alcohols and lipids, are available in the reaction mixture for hydrolysis and condensation reactions which form the final product. In contrast, in the case of G-CE-nFe, glucose is the only compound which is hydrolyzed and is available for condensation and polymerization reactions. Glucose has been deeply studied as a starting material for producing carbon materials through HTC. It is well known that when treating glucose under temperatures of 170-300 ºC, micro-carbon spheres of sizes 0.25-8 μm depending on the conditions applied are formed[29]. Conversely, the reactions undertaken by OMW through HTC process are suggested to be very complex and a clear scheme has not been reported, since several compounds are implied. Interestingly, in Wang et al.'s work[30], in which a mixture of melamine and glucose was used as a carbonaceous source, a material similar to the OMW-CE-nFe was obtained. The nZVI was encapsulated in nanocarbon spheres of diameter of 50-100 nm. The nanomaterial had also high iron content (≈30%), although the surface area of the material was only 18 m^2/g. Apart from melamine, other works have shown to be able to produce nanoparticles through HTC method, although not containing iron. In Atchudan et al.'s recent work (2017), the fruit extract from Chionanthus retusus, which is rich in phenolic compounds and polysaccharides, was used to synthesize N/C nanospheres of very low size (3-7 nm) through HTC (180ºC, 6 h) [31]. Similarly, Yan et al. (2015) synthesized carbon nanoparticles of 10-25 nm from wood derived sugars with HTC treatment at temperatures of 160-180ºC during 8 h [32]. Thus, it is concluded that depending on the

carbonaceous source used for the HTC process, different structures can be obtained for the final material, and OMW has proven to be able to produce nanocarbon spheres of very low size, thus being a promising raw material for the green synthesis of nanomaterials.

Effect of HTC conditions on synthesized CE-nFe

Temperature effect

Changing the temperature of the reaction had a slight but not important effect on the amount of CE-nFe synthesized and the iron percentage incorporated into the sample, as seen in Table 1. The amount of nanoparticles obtained decreased with the temperature due to the higher degree of carbonization. However, the difference between the highest and the lowest value (at 180 and 275ºC, respectively) was 0.8 g, which corresponded to only 10 % of the average value. The iron content incorporated into the material increased with temperature up to 225ºC and then it remained constant, but this was ascribed to the consequent decrease of the sample weight. The results revealed that temperatures above 200ºC were sufficient in order to obtain 100% incorporation of iron (3.16 g) into the final material.

On the contrary, the surface area of the material calculated by the BET analysis presented a strong variation with temperature (see Table 1). The surface area showed a maximum value at a reaction temperature of 225ºC, when its value almost doubled the one at 180ºC (190 m^2/g vs 108 m^2/g). Taking into account the pore size distribution of the materials obtained by the BJH model (see Figure S6 in Supporting Information), it can be seen that at 200ºC and 250ºC reaction temperatures, the most abundant pore size was 3.8 nm. At 180ºC and 250ºC, the distribution was also centered at the same value of pore size, but with a lower content. At the highest temperature evaluated (275ºC), the pore size distribution moved towards higher pore sizes (8.6 nm). Considering that the sequestration of some heavy metals relies on the adsorption capacity of the iron nanoparticles, the total surface area is an important property. Consequently, it is not beneficial to increase the HTC reaction temperature higher than 225ºC according to the surface area results.

Another effect observed in the final material as a result of the change in temperature was the crystallinity. As shown in XRD results (see Figure S7 in Supporting Information), while at 180ºC the material was amorphous, at 200ºC the characteristic peaks of maghemite at 2θ values of 35.7, 57.2 and 62.8º were visible, and became higher at 275ºC.

Effect of reaction time

The duration of the HTC reaction had a similar effect as the temperature in the solid production (see Table 1). The higher the reaction time, the higher the carbonization of the material and thus, the lower the amount of solid obtained. The iron content of the solid consequently increased with the reaction time due to the decrease in the total sample weight.

The analysis of the BET surface area of the samples showed a maximum at a reaction time of 3 h, as seen in Table 1. This was consistent with the pore volume and pore size distribution obtained by the BJH model (see Figure S8 in Supporting Information). Although the three samples displayed a single modal pore size distribution centered at 3.8 nm, at the reaction time of 3 h the proportion of pores at that size was higher. Regarding the XRD analysis of the sample, the crystallinity of the material increased with reaction time, as shown in Figure S9 of Supporting Information.

Effect of initial iron concentration

When increasing the nFe/nC_i, there was a subsequent increase in both the solid production and the Fe percentage in the final material, as seen in Table 1. The iron mass incorporated into the nanomaterial steadily increased with the amount of iron precursor added. This was to be expected, as more Fe available at the start increased the possibility for a higher incorporation of Fe in the final product. Looking at the data at Table 1, it can be seen that the iron incorporated into the final nanomaterial was always the stoichiometric put into the reaction, i.e., all the iron added as iron nitrate to the reactor was precipitated in the OMW-CE-nFe. The solid production

also increased with the increase of nFe/nC_i ratio, which was due in part to the higher amount of iron precipitated in each experiment. But it is more interesting to note that the carbonaceous mass also increased with nFe/nC_i ratio. Although the initial mass of OMW was the same for all the experiments, the increase in iron resulted in a higher carbon production. Consequently, the recovery of the reaction, defined as the carbonaceous material precipitated through HTC divided by the initial carbon content, could be maximized by increasing the nFe/nC_i ratio.

Regarding the iron percentage in the produced OMW-CE-nFe (nFe/nC_p), it increased linearly until 0.2 $molFe/molC_i$, above which it remained constant (see Table 1). This suggests that the amount of carbon encapsulating the iron decreased when more Fe precursor was added up to 0.2 $molFe/molC_i$, above which the level of coating remained uniform. This was consistent with TEM images of the nanoparticles (see Figure S10 at Supporting Information). At the initial molar relationship Fe/C of 0.01, a wide layer of carbon covered the iron nanoparticles, which were difficult to be distinguished inside the carbon structure due to a low precipitation. However, when increasing nFe/nC_i to 0.05, the nanoparticles precipitated, having an average size of 4.4±0.6 nm, and they were also encapsulated by a thin coating (<1 nm) of carbon. At nFe/nC_i = 0.25, the structure of the nanomaterial was similar, but the size of the iron nanoparticles increased to 9.7±1.5 nm and the carbon coating was such thinner that it was difficult to distinguish it in the TEM images.

The BET surface area of the solid displayed an optimum value at nFe/nC_i = 0.05, which gave the highest surface area (Table 1). At lower ratios, the iron content was not enough to produce the desired structure of the material, as evidenced by TEM and SEM images (see Figure S10 and S11 in Supporting Information). For higher ratios, the large iron loading produced an increase in the nanoparticles sizes as shown in TEM and SEM images and a more crystalline structure. Consequently, the surface area diminished in these samples. Indeed, at nFe/nC_i = 0.25 (sample P17) there were some structures of bigger sizes (150 nm length x 58 nm width) with low carbon content (2.6%) and highly crystalline (see Figure S12 in Supporting Information), which produced a decrease in the surface area available. The increase of crystallinity with the

initial molar ratio nFe/nC_i was also showed by XRD (see Figure S11 in Supplementary Information). At nFe/nCi = 0.01 the sample was completely amorphous, as any crystalline peak was observed. At nFe/nCi = 0.05, the characteristic peaks of γ-Fe_2O_3 (30.3, 35.6º, 43.6, 57.9º, 62.5º) were detected, and at nFe/nCi = 0.15 the same peaks were detected but with a higher magnitude. The pore volume and pore size distribution of the samples calculated by the BJH method (see Figure S13 at Supporting Information), also showed that the highest pore volume was obtained at nFe/nC_i = 0.05, again confirming that this was the optimal value for this parameter.

Post-treatment of OMW-CE-nFe

The TG analysis of the OMW-CE-nFe under nitrogen atmosphere (see Figure S14 in Supporting Information) revealed a sharp weight loss between 600ºC and 800ºC, which can be ascribed to the reduction of ferric iron to zero valent iron and to the graphitization of the carbon. Thus, the post-treatment of the OMW-CE-nFe under nitrogen atmosphere to increase the ZVI content was studied within this temperature range. The results showed that the post-treatment produced an increase in the total iron percentage in the nanomaterial, as shown in Table 2. This was to be expected, since at high temperatures carbon is being converted to CO and CO_2, thus increasing the iron content of the samples. Furthermore, the post-treatment of the samples was successful in increasing the ZVI content. The ZVI increased from 4.5% to 6.6, 10.0 and 15.5 % after the treatment at 600, 700 and 800ºC respectively during 3 h. This was corroborated by XRD patterns shown in Figure S15 of Supporting Information. Before the post-treatment, only the peak of γ-Fe_2O_3 was detected by XRD. However, after the post-treatment at 600ºC and 800ºC the characteristic peaks of bcc Fe(0) at 44.7º and 65.1º were observed and were more intense at the treatment temperature of 800ºC. The sample showed to contain also iron carbide, which had been detected also by Wang et al. when using a mixture of melamine and glucose as starting materials[30]. At 800ºC, it is interesting to notice that crystalline carbon (lonsdaleite) was identified by XRD. Lonsdaleite is known to be synthesized by heating and compression of graphite.

Table 2. Properties of the sample P4 (200ºC, $nFe/nC_i = 0.05$, 3 h,) after the post-treatment. Post-treatment time was set to 3 h for all the samples.

Sample	Post-treatment temperature (ºC)	BET surface area (m^2/g)	% Fe in sample	$\%Fe^0$ of total Fe
P4	-	176	42.5	10.6
P4_N600	600	195	53.0	12.4
P4_N700	700	219	56.4	21.1
P4_N800	800	161	73.1	23.9

It was evidenced by TEM images (Figure 2) that the structure of the nanomaterials was slightly modified after the post-treatment. Some of the iron sintered to higher particle sizes of 46±22 nm (Figure 2a) and they were less aggregated and better distributed into the carbon. Another interesting thing to remark is that when applying the post-treatment temperature of 800ºC, graphitic layers of carbon were observed surrounding the iron nanoparticles (Figure 2b). Although the peak of graphitic carbon was not observed at XRD analysis, the measurement of the distance between the layers of crystalline carbon matched with the one of graphite (0.335 nm). Moreover, the presence of lonsdaleite in the nanomaterial treated at 800ºC further suggested the presence of graphite. The iron nanoparticles encapsulated with graphitic carbon have shown in the literature interesting properties as catalysts for efficient hydrogen evolution[33] and Fischer-Tropsch synthesis[34,35] Thus, the work presented here could serve as a sustainable and low-cost method of synthesizing this kind of material with very interesting applications.

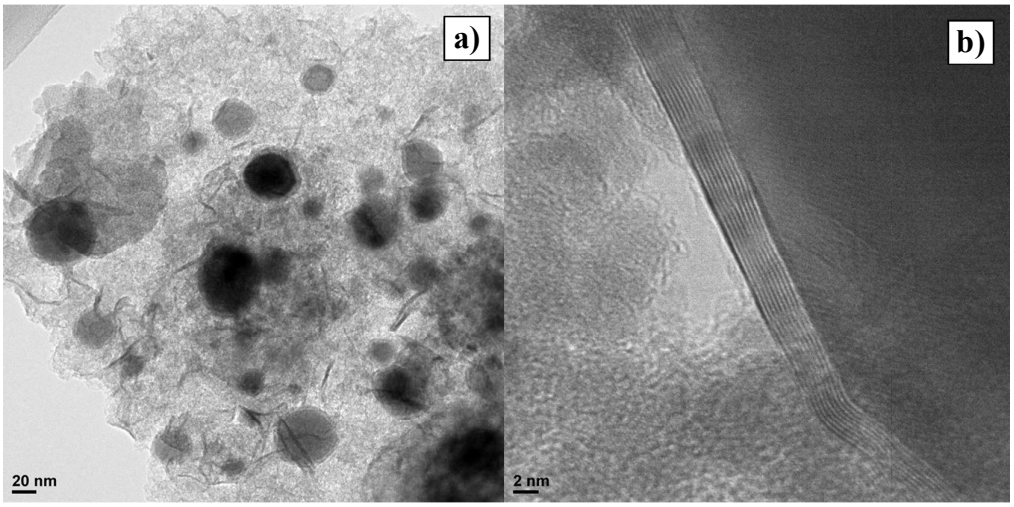

Figure 2. TEM images of the sample P4 (200ºC, nFe/nC_i = 0.05, 3 h) after the post-treatment with nitrogen at high temperatures. a) sample treated at 600ºC; b) detail of the graphitic carbon encapsulating the iron nanoparticles in the sample treated at 800ºC.

Regarding the BET surface area of the nanomaterials, it increased with the post-treatment temperature up to 700ºC, at which it displayed 219 m^2/g (see Table 2). However, at 800ºC, the surface area diminished to 161 m^2/g, which is even lower than the initial surface area of the OMW-CE-nFe before the post-treatment. This can be ascribed to the fact that at 800ºC the carbon becomes crystalline, presenting then a lower surface area, as evidenced by XRD and TEM analysis.

One question of interest of the obtained OMW-CE-nFe after the post-treatment is if the nZVI particles are protected against oxidation by the carbon layer. With this objective, the particles were subjected to a specific program with the TG analyzer to determine their response to the contact to an oxidant atmosphere (see Figure S16 in Supporting Information). Results showed no oxidation of the nanoparticles after 15 hours of contact with air at 25ºC, as the sample weight did not show any increase that would have been ascribed to the formation of oxides in nZVI surface. Thus, it is assumable to affirm that the carbon layer was able to protect the nanoparticles against oxidation.

Application of OMW-CE-nFe in heavy metal removal

The encapsulated particles (CE-nFe, CE-nFe-P600) together with nZVI and AC-P600 were tested for their application in heavy metal remediation of contaminated water. The objective was to elucidate if the encapsulated nanoparticles were able to avoid the aging effect displayed by conventional nZVI observed in a previous study [9], consisting of the delivery of some of the heavy metal cations back to water. The evolution of the heavy metal cations in the aqueous solution during reaction time is shown in Figure 3, and the final removal percentage achieved by each of the materials is shown in Table S3 of Supporting Information. It can be seen in Figure 3 that conventional nZVI and CE-nFe-P600 were the ones that achieved the highest degradation efficiencies. Conversely, AC-P600 was the material that showed the lowest removal efficiency, being negligible for Ni and Zn and only of 1.5% for Cd. Thus, it was corroborated that the carbon produced by HTC from glucose and activated at 600ºC under nitrogen atmosphere did not have sufficient adsorption capacity to remove the heavy metals and that the presence of iron was needed. In the case of CE-nFe, although the removal efficiencies were higher than with AC-P600, they were much lower than with CE-nFe-P600. This is suggested to be due to the lower ZVI content of CE-nFe (4.5%) compared to CE-nFe-P600 (15.5%), and also to its lower surface area.

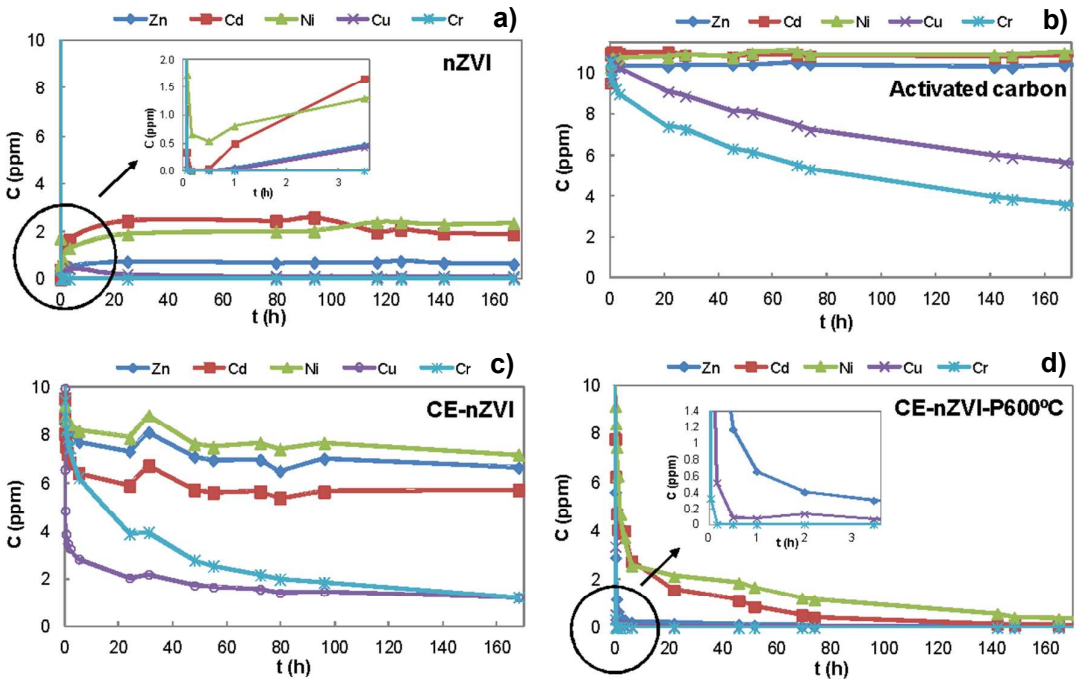

Figure 3. Removal of heavy metal cations with time, using: a) conventional nZVI; b) AC-P600; c) OMW-CE-nFe; d) OMW-CE-nFe-P600. Reaction conditions: C_{i0} = 10 ppm, pHo = 4.7, $C_{Fe,0}$ = 1g/L (except for AC-P600 in which the loading was 2.1 g/L). OMW-CE-nFe used was sample P4 (200ºC, nFe/nC_i = 0.05, 3 h).

Regarding the comparison between conventional nZVI and CE-nFe-P600, while at short reaction times nZVI eliminated the heavy metals from the aqueous solution with high yields (degradation > 99.9 % for Zn, Cd, Cu and Cr; and 93.4% for Ni), at extended periods the contaminants started to be released back to water. This behavior is ascribed to the oxidation of nZVI at long reaction times [9]. However, in the case of the encapsulated nanoparticles, the delivery of the heavy metal cations was not produced, as shown in Figure 3. On the contrary, the percentage of removal increased with the time of application of the nanoparticles until degradations greater than 99% were obtained for all the elements except for Ni, which had a removal efficiency of 97%. In the case of the conventional nZVI, the final degradation percentages of the contaminants were only 94.0, 81.1, 76.5, 99.3, 100 % for Zn, Cd, Ni, Cu and

Cr respectively. Therefore, it is concluded that, for applications in which the reaction times are long, such as the remediation of contaminated soils or aquifers, the encapsulated nZVI could avoid the release of the contaminants back to water that is observed when nZVI particles are employed. At the view of the results, the mechanism by which CE-nFe remove the heavy metals is suggested to involve two steps: the first one corresponds to the adsorption of the heavy metals in the carbon layer, which is a slow step; and the second one consists of the reduction of some of the heavy metals (Cr^{6+}, Cu^{2+}, Ni^{2+}) by metallic iron and its surface complexation with the iron oxide. However, the mechanism of removal of heavy metals is beyond the aim of this paper, which intends to make a preliminary study of the effectiveness of the CE-nFe in avoiding the aging effect of conventional nZVI. We believe that the study of the mechanism of removal of the heavy metals and the study of more applications of this kind of material are interesting issues for future works.

ACKNOWLEDGEMENTS

We would like to acknowledge the Unity of Research Technical Services from the University of Alicante for their help in the analysis performed in this study, especially to Dr. Cristina Almansa for her help with TEM analysis and Dr. Ion Such for his support with pore size distribution calculations. Financial support for this work was given by the University of Alicante (UAFPU2013-5791).

SUPPORTING INFORMATION

OMW characterization, TEM and SEM images, Nitrogen adsorption/desorption isotherms, Pore size distribution of samples, XRD patterns, TG, Removal efficiencies of heavy metals.

REFERENCES

1. Yan, W.; Lien, H. -.; Koel, B. E.; Zhang, W. -. Iron nanoparticles for environmental clean-up: Recent developments and future outlook. *Environ. Sci. Process. Impacts* **2013**, *15*, 63-77.

2. Crane, R. A.; Scott, T. B. Nanoscale zero-valent iron: Future prospects for an emerging water treatment technology. *J. Hazard. Mater.* **2012**, *211-212*, 112-125.

3. Fu, F.; Dionysiou, D. D.; Liu, H. The use of zero-valent iron for groundwater remediation and wastewater treatment: A review. *J. Hazard. Mater.* **2014**, *267*, 194-205.

4. Bezbaruah, A. N.; Krajangpan, S.; Chisholm, B. J.; Khan, E.; Elorza Bermudez, J. J. Entrapment of iron nanoparticles in calcium alginate beads for groundwater remediation applications. *J. Hazard. Mater.* **2009**, *166*, 1339-1343.

5. Zhang, W. -. Nanoscale iron particles for environmental remediation: An overview. *J. Nanopart. Res.* **2003**, *5*, 323-332.

6. Sun, H.; Zhou, G.; Liu, S.; Ang, H. M.; Tadé, M. O.; Wang, S. Nano-Fe0 encapsulated in microcarbon spheres: Synthesis, characterization, and environmental applications. *ACS Appl. Mater. Interfaces* **2012**, *4*, 6235-6241.

7. He, F.; Zhao, D. Manipulating the size and dispersibility of zerovalent iron nanoparticles by use of carboxymethyl cellulose stabilizers. *Environ. Sci. Technol.* **2007**, *41*, 6216-6221.

8. Han, Y.; Yang, M. D. Y.; Zhang, W.; Yan, W. Optimizing synthesis conditions of nanoscale zero-valent iron (nZVI) through aqueous reactivity assessment. *Front. Environ. Sci. Eng.* **2015**.

9. Calderon, B.; Fullana, A. Heavy metal release due to aging effect during zero valent iron nanoparticles remediation. *Water Res.* **2015**, *83*, 1-9.

10. Crane, R. A.; Scott, T. The removal of uranium onto carbon-supported nanoscale zero-valent iron particles. *J. Nanopart. Res.* **2014**, *16*.

11. Liu, H.; Xu, J.; Li, Y.; Li, Y. Aggregate nanostructures of organic molecular materials. *Acc. Chem. Res.* **2010**, *43*, 1496-1508.

12. Zhu, X.; Liu, Y.; Qian, F.; Zhou, C.; Zhang, S.; Chen, J. Preparation of magnetic porous carbon from waste hydrochar by simultaneous activation and magnetization for tetracycline removal. *Bioresour. Technol.* **2014**, *154*, 209-214.

13. Sevilla, M.; Fuertes, A. B. Chemical and structural properties of carbonaceous products obtained by hydrothermal carbonization of saccharides. *Chem. Eur. J.* **2009**, *15*, 4195-4203.

14. Hoch, L. B.; Mack, E. J.; Hydutsky, B. W.; Hershman, J. M.; Skluzacek, J. M.; Mallouk, T. E. Carbothermal synthesis of carbon-supported nanoscale zero-valent iron particles for the remediation of hexavalent chromium. *Environ. Sci. Technol.* **2008**, *42*, 2600-2605.

15. Sunkara, B.; Zhan, J.; He, J.; McPherson, G. L.; Piringer, G.; John, V. T. Nanoscale zerovalent iron supported on uniform carbon microspheres for the in situ remediation of chlorinated hydrocarbons. *ACS Appl. Mater. Interfaces* **2010**, *2*, 2854-2862.

16. Roig, A.; Cayuela, M. L.; Sánchez-Monedero, M. A. An overview on olive mill wastes and their valorisation methods. *Waste Manage.* **2006**, *26*, 960-969.

17. Azbar, N.; Bayram, A.; Filibeli, A.; Muezzinoglu, A.; Sengul, F.; Ozer, A. A review of waste management options in olive oil production. *Crit. Rev. Environ. Sci. Technol.* **2004**, *34*, 209-247.

18. Vlyssides, A. G.; Loizides, M.; Karlis, P. K. Integrated strategic approach for reusing olive oil extraction by-products. *J. Clean. Prod.* **2004**, *12*, 603-611.

19. Hoag, G.E.; Collins, J.B.; Holcomb, J.L.; Hoag, J.R.; Nadagouda, M.N.; Varma, R.S. Degradation of bromothymol blue by 'greener' nano-scale zero-valent iron synthesized using tea polyphenols. *J. Mater. Chem.* **2009**, 19, 8671-8677.

20. Huang, L.; Weng, X.; Chen, Z.; Megharaj, M.; Naidu, R. Green synthesis of iron nanoparticles by various tea extracts: Comparative study of the reactivity. *Spectrochim. Acta Part A Mol. Biomol. Spectrosc.* **2014***, 130*, 295-301.

21. Shahwan, T.; Abu Sirriah, S.; Nairat, M.; Boyacı, E.; Eroğlu, A.E.; Scott, T.B.; Hallam, K.R. Green synthesis of iron nanoparticles and their application as a Fenton-like catalyst for the degradation of aqueous cationic and anionic dyes. *Chem. Eng. J.* **2011**, 172, 258-266.

22. Smuleac, V.; Varma, R.; Sikdar, S.; Bhattacharyya, D. Green synthesis of Fe and Fe/Pd bimetallic nanoparticles in membranes for reductive degradation of chlorinated organics. *J. Membr. Sci.* **2011**, 379, 131-137.

23. Hider, R.C.; Liu, Z.D.; Khodr, H.H. Metal Chelation of Polyphenols. *Methods Enzymol.* **2001**, 335, 190-203.

24. Symonowicz, M.; Kolanek, M. Flavonoids and their properties to form chelate complexes. *Biotechnol Food Sci*. **2012**, 76, 35-41.

25. Poerschmann, J.; Baskyr, I.; Weiner, B.; Koehler, R.; Wedwitschka, H.; Kopinke, F. -. Hydrothermal carbonization of olive mill wastewater. *Bioresour. Technol.* **2013***, 133*, 581-588.

26. Roig, A.; Cayuela, M. L.; Sánchez-Monedero, M. A. An overview on olive mill wastes and their valorisation methods. *Waste Manage.* **2006***, 26*, 960-969.

27. Yu, G.; Sun, B.; Pei, Y.; Xie, S.; Yan, S.; Qiao, M.; Fan, K.; Zhang, X.; Zong, B. FexOy@C spheres as an excellent catalyst for Fischer-Tropsch synthesis. *J. Am. Chem. Soc.* **2010***, 132*, 935-937.

28. Poerschmann, J.; Weiner, B.; Baskyr, I. Organic compounds in olive mill wastewater and in solutions resulting from hydrothermal carbonization of the wastewater. *Chemosphere* **2013***, 92*, 1472-1482.

29. Titirici, M. -.; Antonietti, M. Chemistry and materials options of sustainable carbon materials made by hydrothermal carbonization. *Chem. Soc. Rev.* **2010***, 39*, 103-116.

30. Wang, Y.; Sun, H.; Duan, X.; Ang, H. M.; Tadé, M. O.; Wang, S. A new magnetic nano zero-valent iron encapsulated in carbon spheres for oxidative degradation of phenol. *Appl. Catal. B Environ.* **2015***, 172-173*, 73-81.

31. Atchudan, R; Edison T.N.J.I.; Chakradhar D.; Perumal S.; Shim J.-.; Lee Y.R.. Facile green synthesis of nitrogen-doped carbon dots using Chionanthus retusus fruit extract and investigation of their suitability for metal ion sensing and biological applications. *Sens Actuators, B Chem.* **2017**, *246*, 497-509.

32. Yan, Q; Street, J.; Yu, F. Synthesis of carbon-encapsulated iron nanoparticles from wood derived sugars by hydrothermal carbonization (HTC) and their application to convert bio-syngas into liquid hydrocarbons, *Biomass Bioenergy*. **2015**, *83*, 85-95.

33. Tavakkoli, M.; Kallio, T.; Reynaud, O.; Nasibulin, A. G.; Johans, C.; Sainio, J.; Jiang, H.; Kauppinen, E. I.; Laasonen, K. Single-Shell Carbon-Encapsulated Iron Nanoparticles: Synthesis and High Electrocatalytic Activity for Hydrogen Evolution Reaction. *Angew. Chem. Int. Ed.* **2015***, 54*, 4535-4538.

34. Qin, H.; Zhou, Y.; Bai, J.; Zhu, B.; Ni, Z.; Wang, L.; Liu, W.; Zhou, Q.; Li, X. Lignin-derived thin-walled graphitic carbon-encapsulated iron nanoparticles: growth, characterization and applications. *ACS. Sustain. Chem. & Eng.*. **2017***, 5 (2)*, 1917-1923.

35. Qin, H.; Wang, B.; Zhang, C.; Zhu, B.; Zhou, Y.; Zhou, Q. Lignin based synthesis of graphitic carbon.encapsulated iron nanoparticles as effective catalyst for forming lower olefins via Fischer-Tropsch synthesis. *Catal. Commun.* **2017***, 96*, 28-31.

TOC/ABSTRACT: For Table of Contents Use Only

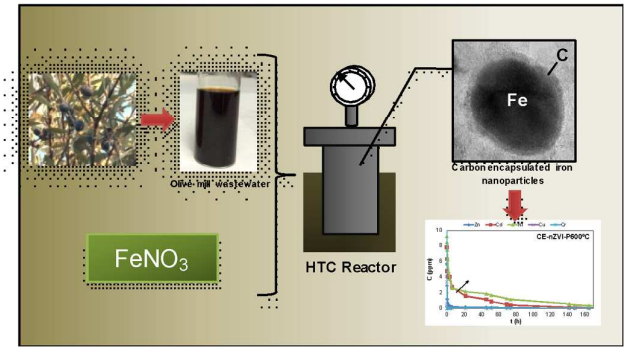

SYNOPSIS: In this work, a sustainable route of synthesizing carbon encapsulated nZVI using a waste stream from the olive oil industry is presented.